Journal of Hydrology: Regional Studies 47 (2023) 101395

Contents lists available at ScienceDirect

Journal of Hydrology: Regional Studies

journal homepage: www.elsevier.com/locate/ejrh

The impact of future hydrology stresses and climate change on submarine groundwater discharge in arid regions: A case study of the Nile Delta aquifer, Egypt

Ismail Abd-Elaty [a,*], Antoifi Abdoulhalik [b], Ashraf Ahmed [b,*]

[a] Department of Water and Water Structures Engineering, Faculty of Engineering, Zagazig University, Zagazig 44519, Egypt
[b] Department of Civil and Environmental Engineering, Brunel University London, Kingston Lane, Uxbridge, Sussex UB83PH, UK

ARTICLE INFO

Keywords:
Sea level rise
Climate change impact
Groundwater abstraction
Saltwater intrusion
Nile Delta aquifer
Arid regions

ABSTRACT

Study region: Climate change is expected to severely impact Egypt's Nile Delta Aquifer (NDA). Despite its large freshwater reservoir, estimated at 400 Billion Cubic metres (BCM), climate-change-induced drivers (drought and sea-level rise) coupled with increasing groundwater over-abstraction will cause a gradual reduction of the available freshwater volume. This study used the numerical model SEAWAT to study the impact of the main hydrogeological and anthropogenic factors on the response of the submarine groundwater discharge (SGD) (i.e., the net fresh seaward groundwater flux) and seawater intrusion (SWI) in the NDA.

Study focus: Five scenarios were examined, including (i) a probable Sea-level rise (SLR), (ii) expected reduction in Nile hydrograph and its branches, (iii) freshwater overpumping, (iv) the combination of reduction in Nile hydrograph and overpumping, and (v) the combination of these scenarios in the years 2030, 2050 and 2070.

New hydrological insights for the region: The results show that the increasing saltwater head due to SLR coupled with a reduction in Nile flow and overpumping ultimately results in the landward shifting of the saltwater within the aquifer. In addition, the resulting salinity increase in the aquifer caused a significant increase in the deterioration of a large quantity of freshwater volume with a subsequent reduction of the SGD. Also, the salt mass variation (SMV) in scenario 5 increased to 7.09%, 10.69%, and 12.99%, while the groundwater discharges variation (SGDV) to the sea declined by 21.90%, 42.38%, and 61.95% in the years 2030, 2050 and 2070, respectively. Moreover, the coastal aquifers required the management of the SGD to keep the balance between the freshwater and saltwater interface. This study is useful for the future planning and water resources management in coastal regions for integrated management of SGD, SWI, and aquifer freshwater storage. Also, the applications of smart measurements of SGD and groundwater salinity are required for coastal aquifers management.

1. Introduction

Groundwater contamination by seawater intrusion (SWI) is a global issue that mainly impacts coastal aquifers because of several factors, including sea-level rise (SLR), reduction in aquifer landside recharge, which results from drought, and freshwater

* Corresponding authors.
E-mail addresses: Eng_abdelaty2006@yahoo.com (I. Abd-Elaty), Ashraf.ahmed@brunel.ac.uk (A. Ahmed).

https://doi.org/10.1016/j.ejrh.2023.101395
Received 1 February 2022; Received in revised form 13 April 2023; Accepted 20 April 2023
Available online 27 April 2023

overexploitation (Abd-Elaty et al., 2022a, 2022b; Abd-Elaty and Polemio, 2023). The Intergovernmental Panel on Climate Change (IPCC) projects a substantial increase in sea level that will continue to threaten coastal aquifers worldwide, with an expected rise of 0.82 m by 2100 (IPCC, 2014, Abd-Elaty et al., 2021a).

Egypt's coastal Nile Delta (ND) is the most area vulnerable to the environmental impact of SLR in the Mediterranean Sea (Sestini, 1989; IPCC et al., 2008). This will exacerbate the aquifer SWI and damage groundwater quality. The expected SLR in the ND region is estimated at 1.84 mm year^{-1}, with an acceleration of 0.084 mm yr^{-2} (Nerem et al., 2018). Recent ground-based measurements and satellite observations suggested accelerating SLR rates, with an average value of 3.30 mm year^{-1} and acceleration is 0.10 mm yr^{-2} (Legeais et al., 2018).

The decline in freshwater recharge into the aquifer resulting from lesser rainfall, associated with excessive groundwater abstraction to match increasing water demand, also greatly exacerbates SWI in the Nile Delta aquifer (NDA). Several fields and numerical modelling studies have simulated and investigated SWI in the NDA (e.g., El-Fayoumi, 1968; Wilson et al., 1979; Darwish, 1994; Morsy, 2009; Nofal et al., 2015). Recently, the possible influence of combined SLR and overpumping on groundwater salinity in the NDA was studied by Sakr et al., (2004), Abd-Elaty et al. (2014, 2019), Engelen et al. (2019), Mabrouk et al. (2019), Abd-Elaty and Zelenakova (2022) and El Shinawi et al. (2022).

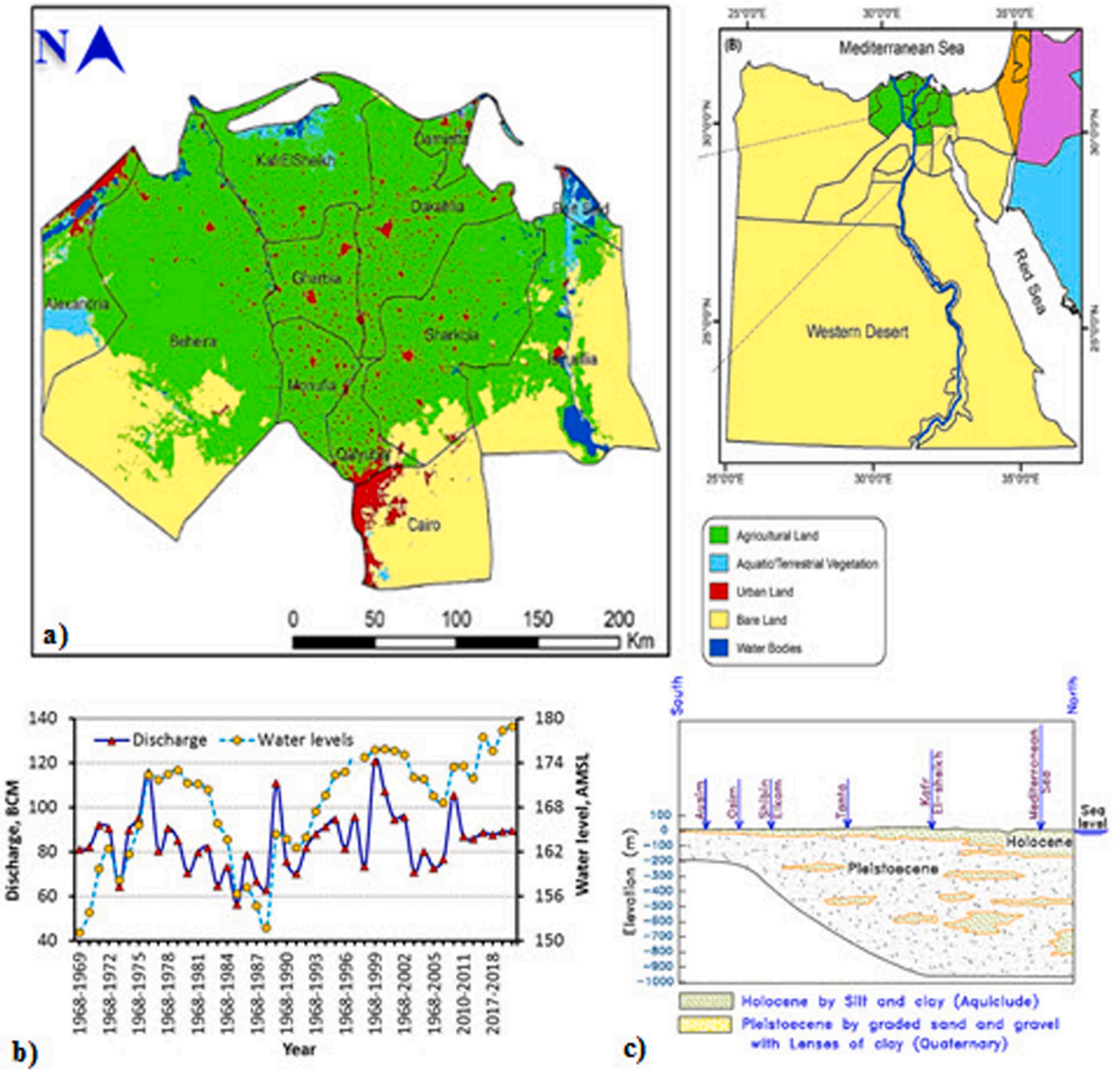

Fig. 1. a) Study area location map of NDA with land use/land cover (LULC) for the nile delta (modified after Radwan et al. (2019), (b) Measured water level and discharge in AHDR, (Amary, 2008; Ramadan et al., 2015; Hossen et al., 2022) (c) Hydrogeological cross-section from South to North of the study area (modified after Negm et al., 2018).

Fresh groundwater over-abstraction leads to the further intrusion of saline water into the aquifer (Abdoulhalik and Ahmed, 2018; Abdoulhalik et al., 2020). Nasar (2004) completed a numerical and laboratory study to investigate the effect of abstracting the brackish water on SWI in the NDA for desalination purposes. Saleh (2009) used MODFLOW to study the application of groundwater abstraction and development activities policies s in the ND region. Wassef and Schüttrumpf (2016) simulated the combined effect of SLR and overpumping using FEFLOW on aquifer salinity in Western ND, Egypt. The low-elevation regions were more impacted by SLR, with SWI shifts landward, covering an area between 1980 and 2870 km^2 from the years 1990–2100. Overpumping was forecasted to damage about 10% of the study area with salinity up to 5000 parts per million (ppm) during the same period from the year 1990–2100.

The current study aims to examine the net seaward groundwater flux to the sea, often called submarine groundwater discharge (SGD), and the aquifer salinity in arid regions by the impact of climate change (CC) and the influence of various hydrological and anthropogenic stresses in the NDA, Egypt. Specifically, climate-related factors will be characterised by SLR and the reduction in the Nile hydrograph and its branches, which often results from recurrent dry seasons. In addition, the fresh groundwater abstraction from the NDA will also be tested. The MODFLOW family model SEAWAT was used in the numerical simulations conducted herein. The codes were applied to investigate the SWI for different scenarios of SLR, reduction of the aquifer recharge, overpumping, and a combination of these cases on the seaward groundwater discharge to the sea. The new positions of the transition zone were determined, and the fresh groundwater storage in the NDA was estimated.

2. Hydrology of Nile Delta reservoir

The climate of the Nile Delta (ND) region is arid (see Fig. 1a), where precipitation is limited and varies between 25 mm $year^{-1}$ to 200 mm $year^{-1}$ along the shoreline of the Mediterranean Sea (RIGW Research Institute for Groundwater, IGW, 1992; Negm et al., 2018; Abd-Elaty and Zelenakova, 2022). The change in the Nile River hydrograph affects the groundwater storage and heads, seaward groundwater discharge, and salinity based on the published historical records. The maximum water supply before Aswan High Dam (AHD) construction reached 21.35 Billion Cubic metres (BCM) in May, while the minimum water supply was reached in January (1.83 BCM). After the construction of the AHD, the water supplies reached the maximum flow value of 8.02 BCM in August, while the minimum flow reached 5.37 BCM in January. Moreover, Fig. 1b presents the measured discharge and water level in Aswan High Dam Reservoir (AHDR) from 1968 to 2021 (Ramadan et al., 2015; Morsy, 2009; Abd-Elaty et al., 2021b; Hossen et al., 2022).

Before the AHD's construction, the ND's groundwater supplies were abstracted to supplement the agricultural water in the irrigation process due to the water resources shortage in the irrigation network's tail ends. The freshwater flowing directly to the sea was estimated at 0.37 BCM in 1958–0.283 BCM in 1962. The reduction in fresh groundwater heads was due to farmers' illegal drilling of new abstraction wells (RIGW Research Institute for Groundwater, 1966; Morsy, 2009).

After the construction of AHD, the groundwater heads increased from years 1957–1984, the groundwater salinity records were enhanced, and the fresh groundwater flow was mitigating SWI. After 1984, the Nile hydrograph declined, leading to extensive groundwater abstraction to overcome the water shortage, which increased groundwater salinity and reduced freshwater flow to the sea. In 1990, the Nile hydrograph increased, and the salinity reduced. In the year 2000, the abstraction wells rates increased for providing the irrigation water for the new agriculture reclamation, which lowered groundwater heads and the flow to the sea, and again raised the salinity in the ND (Sakr et al., 2004; Morsy, 2009; Nofal et al., 2015; Negm et al., 2018; Abd-Elaty and Zelenakova, 2022).

Today, the ND is highly vulnerable to the impacts of CC, including the SLR, erosion, and accretion of the shoreline, reduction in the Nile River hydrograph due to the new upper Nile projects, and excessive freshwater overpumping. All these reasons will affect the aquifer water heads, salinity, and the flux to the sea.

3. Materials and methods

3.1. Middle Nile Delta aquifer (case study area)

The study area is located in the middle part of NDA and is located between the two branches of the Nile River, Damietta and Rosetta. The hydrological boundaries of the study area are the Mediterranean Sea in the north, the Nile River in the south, and its two branches, on the eastern and western sides, respectively (see Fig. 1a). The study domain locates between the latitude 30° 20` and 31° 50'N and longitudes 30° 10'and 31° 35'E. The total area of the middle part of ND is about 9000 km^2, with a coastline length of 170 km and a width of 200 km from south to north, as published by the Ministry of Water Resources and Irrigation (Ministry of Water Resources and Irrigation MWRI, 2013).

3.1.1. Meteorological conditions

The study area's climate is dry with limited precipitation (RIGW Research Institute for Groundwater, IGW, 1992; Morsy, 2009; Abd-Elaty and Zelenakova, 2022). The warmest month in the study area is July, when the average temperature could typically rise to 34.7 °C. On average, the lowest temperature occurs in January when it decreases to 18.9 °C. The highest relative humidity values are recorded in August, November, and December, when it increases to 61%, while the lowest is recorded in May, when it decreases to 46%. The wettest month is December; the precipitation heads could reach up to 5.9 mm, while the driest months are July, August, and September when the precipitation is null (i.e., 0 mm). The highest numbers of rainy days are the month of January by 3.5 days, while the lowest numbers are in July, August, and September by 0 days (https://www.weather-atlas.com/en/egypt/cairo-climate#humidity_relative). The study area evaporation rate ranges from 7 mm day^{-1} in the south to 4 mm day^{-1} in the North

(Morsy, 2009; Abd-Elaty and Zelenakova, 2022).

3.1.2. Hydrogeological

The main body of the NDA is composed of Tertiary and Quaternary deposits. The tertiary aquifer contains deposits of Eocene, Oligocene, Miocene and Pliocene Rocks. Quaternary aquifer covers a large part of the NDA, and includes Holocene and Pleistocene deposits. The aquifer's deposit thicknesses are variable and have different proportions of sand, clay, and gravel (Sallouma, 1983). The maximum Holocene deposits thickness is about 77 m, while the Pleistocene deposits are 700 m thick and have clay lenses (Hefny, 1980) (See Fig. 1c).

The ND region covers by complex networks of irrigation and drainage. These surface water networks are hydraulically connected and interact with the aquifer system (Ministry of Water Resources and Irrigation MWRI, 2013). The NDA is a semi-confined aquifer covering the ND's whole area. The aquifer thickness is about 200 m in the south up to 1000 m in the North (RIGW Research Institute for Groundwater, IGW, 1992). The depth of the groundwater table from the ground surface in the NDA is about 1–2 m in the north, 3–4 m in the middle, and 5 m in the South (RIGW, 2002; Morsy, 2009).

The NDA is a renewable aquifer; the recharge process occurs by downward leakage by excess irrigation water and infiltration of canals, ranging between 0.25 mm day^{-1} and 0.80 mm day^{-1}. Moreover, the recharge also occurs through rainfall during the winter, with the average precipitation reaching 25 mm year^{-1} and inter-aquifer flow to groundwater (RIGW Research Institute for Groundwater, IGW, 1992; Morsy, 2009; Abd-Elaty and Zelenakova, 2022).

The annual abstraction from the NDA gradually increased from 1980 to 2016, at a rate of 0.10 BCM year^{-1}, and reached 0.20 BCM year-1 from 2003 to 2010 (Mabrouk et al, 2013). In 1980, the total abstraction reached 1.60 BCM, and increased up to 2.60 BCM, 3.02 BCM, 4.90 BCM and 7BCM in the years 1991, 1999, 2003, and 2016, respectively (RIGW Research Institute for Groundwater, IGW, 1992; Morsy, 2009; Molle et al., 2016).

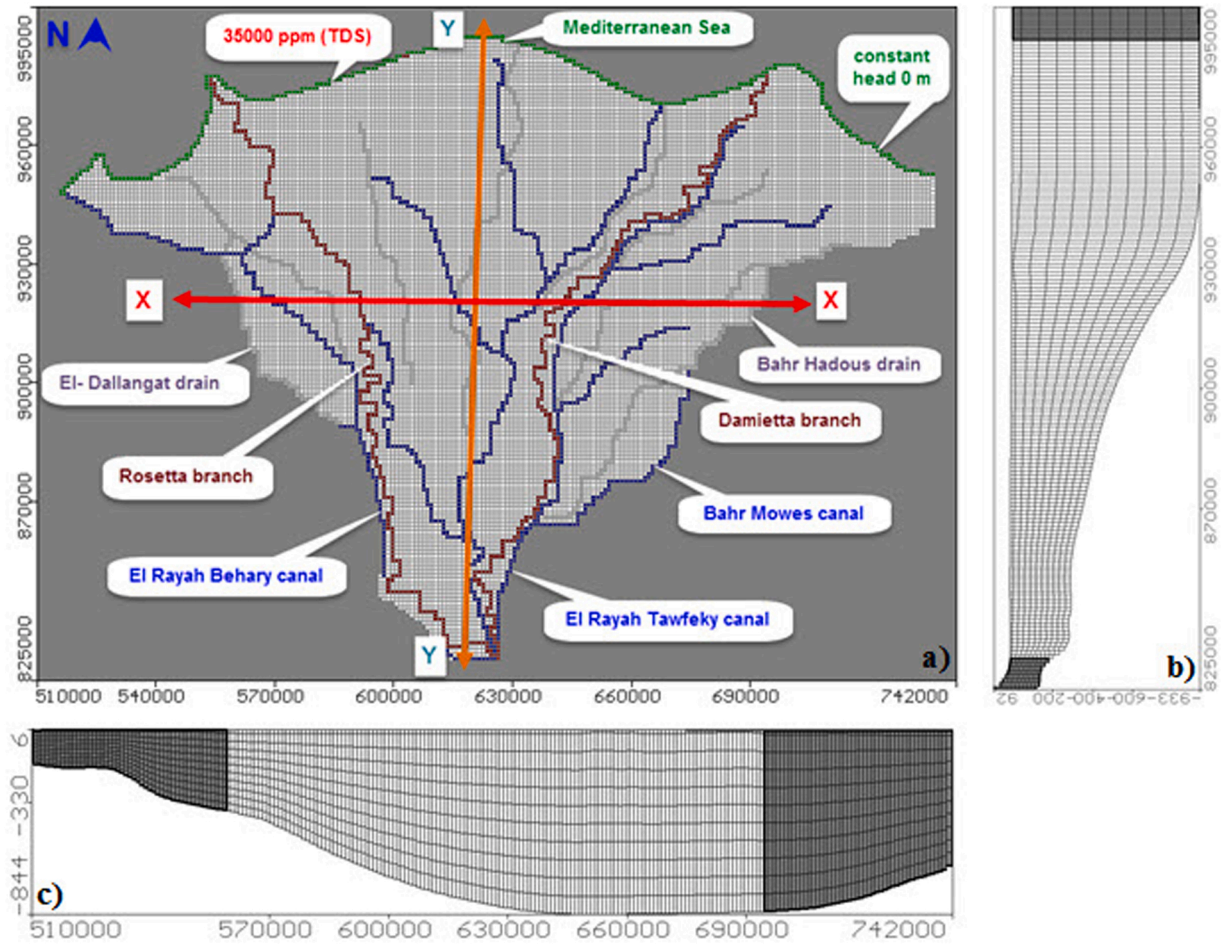

Fig. 2. Nile delta Model for (a) view boundary conditions, (b) Vertical section in x- direction, and (c) vertical section in the y-direction.

3.2. Numerical model description

The SEAWAT numerical code was applied in the NDA. This code simulates the fluid density and viscosity as a function of one or more species of solute (contamination parameters) (Langevin et al., 2007). Also, it is a couple of MODFLOW (Harbaugh et al., 2000) and the code of MT3DMS (Zheng and Wang, 1999). The Variable-Density Flow (VDF) process solves this equation (Guo and Langevin, 2002):

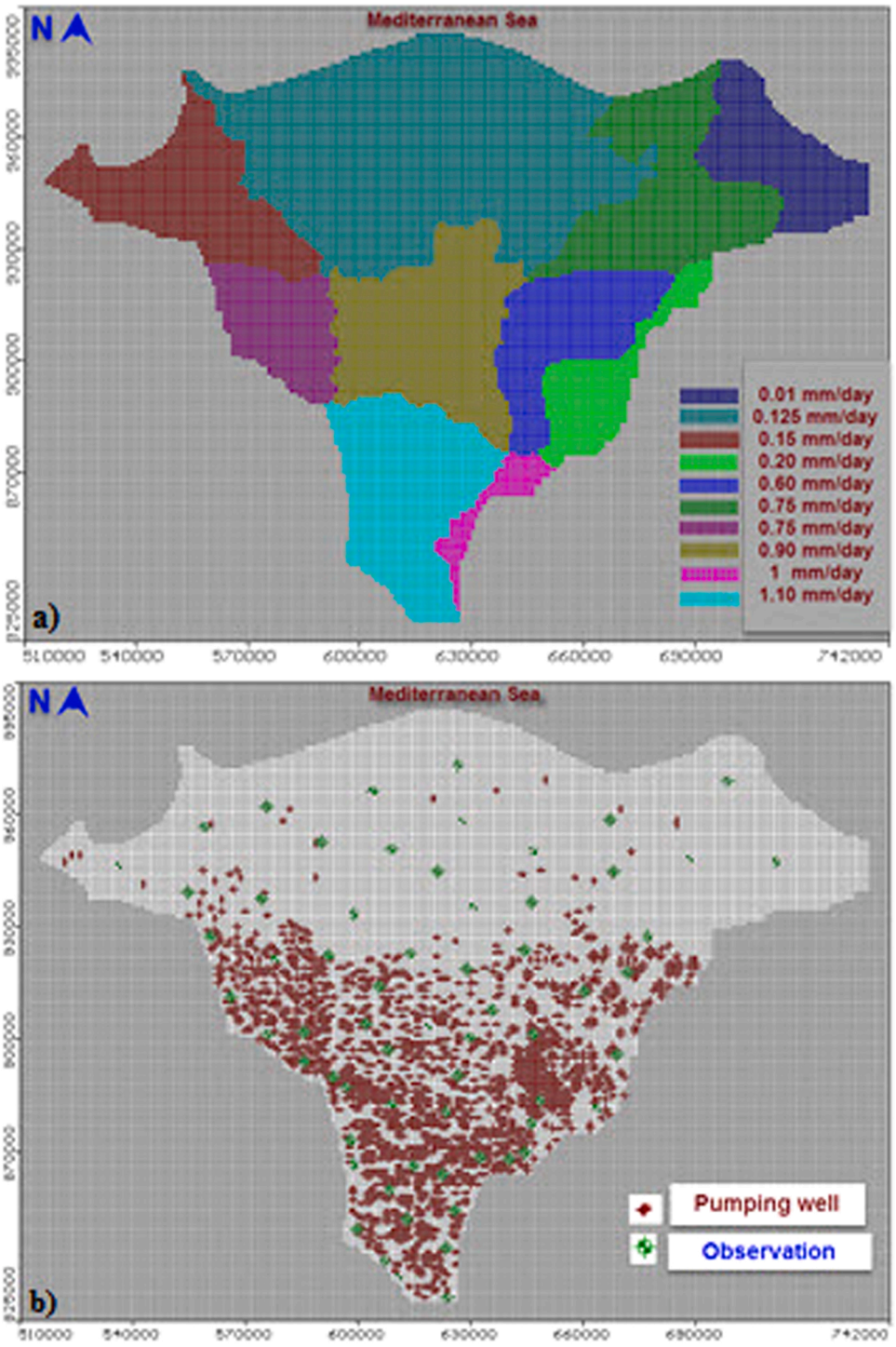

Fig. 3. Nile delta Model for (a) map for the flow to NDA, and (b) map of abstraction and observation wells.

$$\nabla\left[\rho\frac{\mu_o}{\mu}K_o\left(\nabla h_0+\frac{\rho-\rho_o}{\rho_o}\nabla Z\right)\right]=\rho S_{S,0}\frac{\partial h_O}{\partial t}+\theta\frac{\partial\rho}{\partial C}\frac{\partial C}{\partial t}-\rho'_s q'_S \quad (1)$$

The Integrated MT3DMS Transport (IMT) process solves the following equation (Zheng and Wang, 1999):

$$\frac{\partial(\theta C^k)}{\partial t}=\frac{\partial}{\partial x_i}\left(\theta D_{ij}\frac{\partial C^k}{\partial x_j}\right)-\frac{\partial}{\partial x}\left(\theta v_i C^k\right)+q_s C_k^s+\sum R_n \quad (2)$$

Where ρ: the density of saline water [kg m^{-3}]; μ_o: the dynamic viscosity of freshwater [kg m^{-1} sec^{-1}]; μ: the dynamic viscosity of saline water [kg m^{-1} sec^{-1}]; K_0: the hydraulic conductivity [m sec^{-1}]; h_0: the hydraulic head [m]; ρ_o: the fluid density [kg m^{-3}] at the reference concentration; $S_{s,o}$: the specific storage [m^1], t: time [sec]; θ: is porosity [-]; C: the concentration [kg m^{-3}]; q'_s: a source or sink of fluid with a density of ρ_s [sec^{-1}], C^k: the dissolved concentration of species [kg m^{-3}]; *Dij*: the hydrodynamic dispersion tensor [m^2 sec^{-1}]; v_i: the seepage or linear pore water velocity [m sec^{-1}]; C_s^k: the concentration of the source or sink flux for species k [kg m^{-3}]; ΣR_n: the chemical reaction term [kg m^{-3} sec^{-1}].

3.3. Model setup

The study area domain has variable depths ranging from 1000 m to 200 m at the North and South, respectively. The numerical model used 171 rows and 233 columns, with a cell dimension of 1 km^2 (see Fig. 2a). The domain included eleven layers, where layer#1 is the clay cap with a thickness varying from 20 m to 50 m in the south and north, respectively, while layers # 2–11 represent the quaternary aquifer by equal thickness. The clay cap (layer #1) keeps the quaternary aquifer as a semi-confined aquifer. Figs. 2b and 2c show the two vertical cross sections in X and Y directions, respectively.

The flow boundary condition is zero m head above mean sea level (AMSL) along the Mediterranean Sea, which refers to the estimated SLR in the year 2000. This boundary is assigned using the constant head boundary same as for the two branches of the Nile, where the groundwater heads ranged between 13.66 m AMSL for Rosetta branch and 13.17 m AMSL for Domettia branch in the south, to 0.50 m in the north. The river packages within MODFLOW were assigned for the irrigation canals in the study area. El-Rayeah El-Tawfeky canal at the East with starting head varying from 14.80 to 4.30 m (AMSL), Bahr Mowes canal starting head varying from 11.84 m to 4.23 m (AMSL), In the West, El-Rayeah El-Behairy canal was assigned with starting a head range from 16 m to 1.50 m (AMSL). The surface drains are assigned by the MODFLOW drain package with Bahr Hadous in the East starting with surface water levels from 2.50 m in the south to 0.25 m (AMSL) in the North and El- Dallangat drain at the West with the head from 7 m at the south to 0.75 m (AMSL) at the north. The other irrigation canals and drains were assigned to the model, and the surface water levels are sloped from the south to the north, as shown in Fig. 2a (Abd-Elaty et al., 2021c, 2022b).

The contaminant source in NDA is applied using a constant value of 35,000 ppm for the seawater of Total Dissolved Solids (TDS) along the shoreline; the initial concentration of the fresh groundwater was set at 0 ppm, as shown in Fig. 3a (Abd-Elaty, 2014; Abd-Elaty and Zelenakova, 2022).

Table 1
Hydraulic parameters and properties inputs for the model.

Hydraulic Parameters		Symbols	Dimension	Value
Quaternary clay	Vertical hydraulic conductivity	K_V	m day^{-1}	0.01–0.025
	Horizontal hydraulic conductivity	K_h	m day^{-1}	0.10–0.25
	Porosity	n	%	50–60
	Specific storage	S_s	-	10^{-7}
	Specific yield	S_y	-	0.10
Quaternary sand and gravels	Vertical hydraulic conductivity	K_V	m day^{-1}	0.50^{-10}
	Horizontal hydraulic conductivity	K_h	m day^{-1}	5–100
	porosity			12–40%
	Specific storage	S_s	-	5×10^{-3} - 5×10^{-4}
	Specific yield	S_y	-	0.15 – 0.20
Dispersion Parameters		Symbols		Value
Longitudinal dispersivity		α_L	m	250
Lateral dispersivity		α_T	m	25
Vertical dispersivity		α_V	m	2.50
Diffusion coefficient		D*	m^2 day^{-1}	10^{-4}
Hydrological properties		Symbols		Value
Hydraulic conductance	Damietta Branch	C	m^2 day^{-1}	800–500
	Rosetta Branch			800 – 500
	El Rayah El Twafiky			500–350
	El Rayah El Menofy			450 – 300
	Bahr Mowes			300–200
	Bahr Hadous drain			300–200
	Dallangat drain			250–200

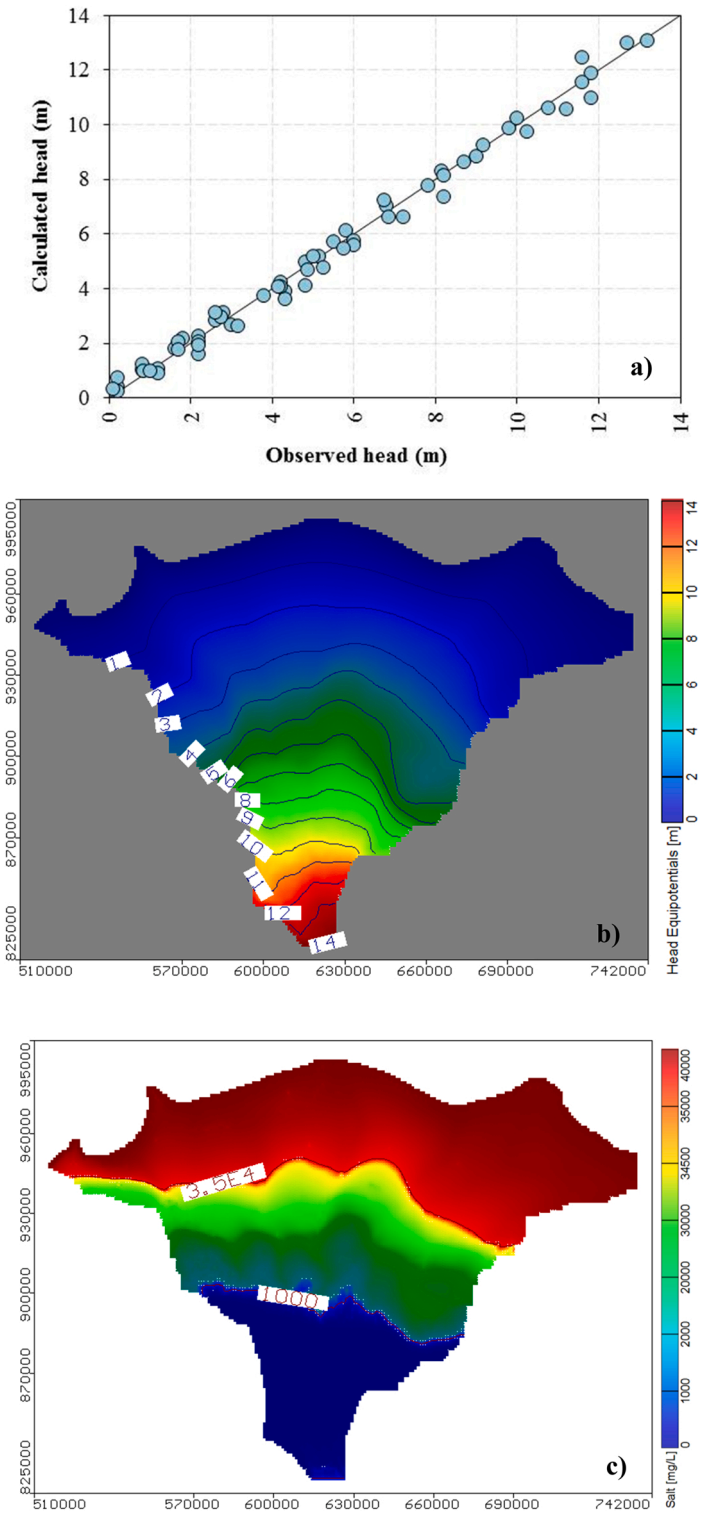

Fig. 4. Calibrated Nile delta model for (a) calculated and observed hydraulic head contour lines, (b) Map of groundwater flow model in the studied aquifer and (c) Map of TDS (output by SEAWAT).

3.4. Model hydraulic parameters and boundary conditions

Extensive studies estimated the aquifer hydraulic parameters. The model input values for these parameters of the current NDA are included in Table 1. The parameters include hydraulic conductivity, specific yield, storage coefficient, transmissivity, and porosity; these parameters are based on previous studies and some calculations using pumping tests (RIGW Research Institute for Groundwater, IGW, 1992; RIGW, 2002; Morsy, 2009; Abd-Elaty et al., 2014; Nofal et al., 2015).

The distribution of aquifer recharge ranges between 0.01 mm day^{-1} in the north to 1.05 mm day^{-1} in the south. The total aquifer recharge reached about 6 × 10^6 m^3 day^{-1} (2.20 BCM year^{-1}). Moreover, two sources of abstraction from groundwater activities in the NDA include the production of drinking water wells and governmental irrigation water wells as presented in Fig. 3a. Fig. 3b shows the distribution of pumping wells in the current study area, which are assigned to the model by each pumping well rate. The total abstraction rate for drinking and irrigation purposes was 4.38E6 m^3 day^{-1} (1.60 BCM yr^{-1}) (Morsy, 2009). The depths of production of governmental irrigation water wells ranged between 80 m and 100 m, while the production of drinking water wells ranged between 120 m and 150 m (Morsy, 2009).

3.5. Model calibration

A total number of 64 observation wells were used in the model calibration. The calibration results showed that the residual groundwater head (difference between the calculated and observed head values) ranged between 0.862 m and − 0.001 m. The residual mean head reached − 0.027 m, which measures the residual average. Also, the absolute residual mean reached 0.284 m, which measures the residuals average magnitude and gives a better calibration indicator than the residual mean. The standard error of estimation of 0.045 m measures the residual variability. The root means squared (RMS) was 0.356 m with a normalisation of 2.64%, which is fitter than the standard RMS. Fig. 4a presents the relationship between the observed and calculated heads, which shows a good correlation. The groundwater head ranged from 14 m AMSL in the south to 0.0 m at the seaside in the North (Fig. 4b). The following equations were used in the calibration process:

$$R_i = X_{cal}\text{-}X_{obs} \tag{1}$$

$$\bar{R} = \frac{1}{n}\sum_{i=1}^{n} R_i \tag{2}$$

$$\left|\bar{R}\right| = \frac{1}{n}\sum_{i=1}^{n} |R_i| \tag{3}$$

$$SEE = \frac{\sqrt{\frac{1}{n-1}\sum_{i=1}^{n}\left(R_i - \bar{R}\right)^2}}{n} \tag{4}$$

$$RMS = \sqrt{\frac{1}{n}\sum_{i=1}^{n} R_i^{\,2}} \tag{5}$$

$$NRMS = \frac{\overrightarrow{RMS}}{(X_{obs})_{\max} - (X_{cal})_{\min}} \tag{6}$$

Where R_i: the residual; $\bar{R}_i$: the residual mean; n: the numbers of data points; $\left|\bar{R}_i\right|$: the absolute residual mean; $\bar{R}_i$: the absolute residual; SEE: the standard error of the estimate; RMS: the root mean squared error; NRMS: normalised root mean squared; Xobs: the observed point results; Xcal: the calculated point results.

After the groundwater flow model calibration and validation, it was then applied to the solute-transport simulation. The SEAWAT results of the TDS in the NDA (layer #6) are presented in Fig. 4c. The salinity distribution assigns an areal view by average thickness of

Table 2
Proposed scenarios for different future years.

Scenarios	Year	Base case (2008)	2030	2050	2070
A	Seal level rise (cm)	0	17.60	35.20	52.80
B	Reduction in Nile flow (%)	0	-7.50	-13	-18.50
	Nile flow (Bm^3 year^{-1})	55.50	51.30	48.20	45.20
	Recharge reduction for study area (Mm^3 year^{-1})	6,000,400	5,550,370	5,220,348	4,890,326
C	Population increasing rate (%)	0	41	102	184
	Egypt population (Million)	79	112	159	225
	50% of population increasing	0	20	51	92
	Abstraction (Mm^3 year^{-1})	4,378,700	5,254,440	6,611,837	8,407,104

about 450 m in the north to 100 m in the south; the vertical view using cross-section is taken in the middle of the aquifer with a length of 150 km and a depth ranging from 200 to 1000 m. The isochlorine at 35,000 ppm and 1000 ppm reached 63.60 km and 101.70 km from the shoreline, respectively, with the transition zone, which is the area between TDS of 35,000 ppm and 1000 ppm, reaching around 38.10 km. The current SEAWAT results were compared with those of Abd-Elaty et al. (2014), and it was found to agree with the observations in the middle cross-section.

3.6. Modelling future scenarios

The model was applied for three future scenarios to investigate their influence on groundwater flow and SWI in the NDA in the years 2030, 2050, and 2070. The scenarios included a sea-level rise estimated by 17.60 cm, 35.20 cm and 52.80 cm relative to the year 2020 (Abd-Elaty et al., 2019); Nile flow reductions of 7.50%, 13%, and 18.50% compared to the base case (the calibrated model), an increase in fresh groundwater abstraction by 20%, 51%, and 92% (Abd-Elaty et al., 2021c) for the years 2030, 2050, and 2070 respectively due to overpopulation; and finally a combination of these scenarios. The proposed different cases are shown in Table 2.

Fig. 5 presents the hydrological cycle for the NDA, including sea level rise (Scenario A), the Reduction in Nile River hydrograph, recharge and return flow (Scenario B), groundwater abstraction (Scenario C), Submarine Groundwater Discharge and saltwater intrusion.

4. Results and discussion

The current section shows the analysis results for the impact of the aquifer hydrological forcing on aquifer groundwater flow and salinity.

4.1. Simulation of groundwater flow for future scenarios

4.1.1. Effect of SLR (Scenario A)

As previously stated, the seawater level in this scenario was raised to 17.60 cm, 32.20 cm, and 52.80 cm in the years 2030, 2050, and 2070, respectively, due to the expected impact of CC. Fig. 6a shows the groundwater head differences (GHD) at the shoreline for the different SLR scenarios. The groundwater head differences, i.e. (H_i-H_o), were calculated to examine the water balance (where H_0 is the initial groundwater head for the baseline case and H_i is the groundwater head for the given scenario). The groundwater heads at the seaside have noticeably increased. As expected, the groundwater heads displayed the maximum rise and reached 17.60 cm, 32.20 cm, and 52.80 cm along the shoreline and decreased gradually towards the landward side. The maximum impacted distance is about 140 km on the land side measured from the shoreline.

4.1.2. Effect of decreasing the Nile flow hydrograph (Scenario B)

The flow to the aquifer based on the reduction in the Nile flow hydrograph by 7.50%, 13%, and 18.50% due to the future impact of CC in the years 2030, 2050, and 2070, respectively, compared to the base case (Fig. 6b). The results show that the groundwater heads dropped down following the reduction of the Nile flow resulting from the decrease in the aquifer recharge. Compared with the base case, the maximum GHD was recorded at 100 km away from the shoreline and reached 0.48 m, 0.85 m, and 1.24 m in the years 2030, 2050, and 2070, respectively.

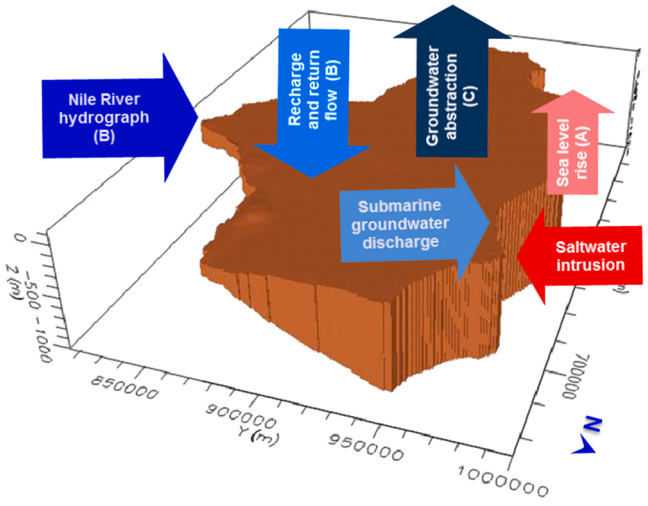

Fig. 5. 3D for Nile delta aquifer for aquifer hydrological forcing.

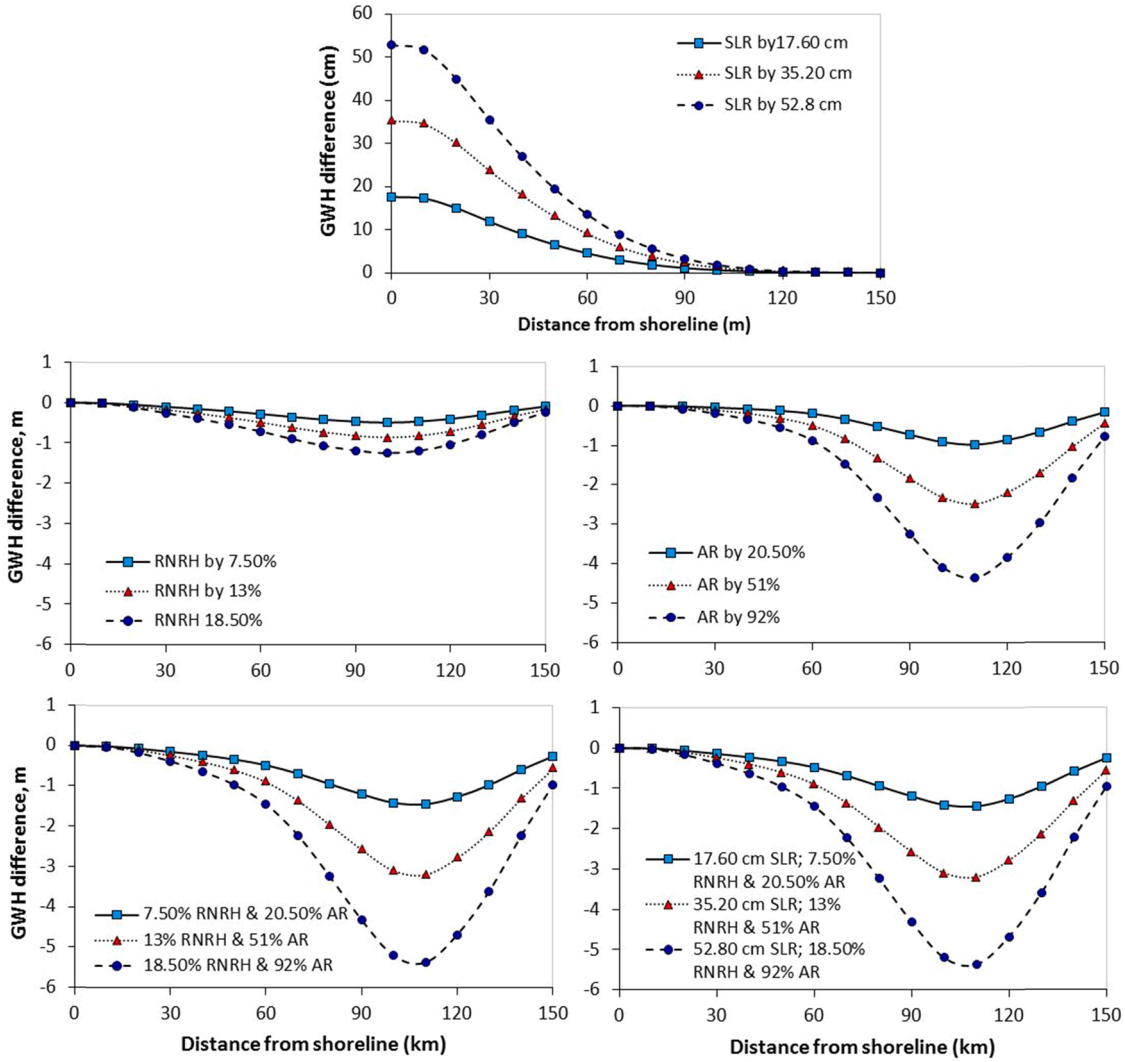

Fig. 6. Relation between piezometric head difference and distance from the shoreline for the forecasted scenarios in the investigated aquifer, (a) Different SLR (scenario A), (b) Different reduction in Nile River hydrograph (RNRH) (scenario B), (c) Different abstraction rates (AR) (scenario C), (d) Different reduction in Nile hydrograph (RNH) and abstraction rates (AR) (scenario D) and (e) Combination of A, B and C scenarios (scenario E).

4.1.3. Effect of increasing abstraction rates (Scenario C)

This scenario assesses the impact of over-abstraction by production wells on groundwater flow in the Nile Delta region. Fig. 6c shows the groundwater head response to an increase of groundwater pumping by 20%, 51%, and 92% in the years 2030, 2050, and 2070, respectively, compared with the current abstraction rates. The results show that the groundwater heads decreased with increasing abstraction rates. Based on the baseline case, the differences in groundwater heads reached 0.98 m, 2.48 m, and 4.35 m at a distance of 110 km from the shoreline, respectively.

4.1.4. Combined effect of decreasing the Nile hydrograph and increasing abstraction rates (Scenario D)

In this scenario, the combined effect was studied by decreasing the flow to the aquifer due to the reduction of the Nile hydrograph by 7.50%, 13%, and 18.50% and increasing the abstraction wells rates by 20%, 51%, and 92% in the years 2030, 2050, and 2070, respectively, relative to the base case. The results of this scenario indicated that the groundwater heads dropped, and the GHD reached 1.44 m, 3.19 m, and 5.37 m at a distance of 110 km from the shoreline, as shown in Fig. 6d.

4.1.5. Effect of combined scenarios (Scenario E)

The combination of scenarios A, B, and C induced a further drop in the groundwater heads, as shown in Fig. 6e. The results indicated that the groundwater head rose in the upward direction in the north due to the increase in SLR, while it decreased in the south due to the concentration of the abstraction wells and irrigation systems. The differences in groundwater heads reached 1.43 m, 3.18 m, and 5.35 m at a distance of 110 km from the shoreline in the years 2030, 2050, and 2070, respectively. Moreover, the effect of

SLR was found to be negligible at a distance of 140 km from the shoreline, where the GHD reached about 1.50 cm, 2.60 cm, and 3.90 cm in the years 2030, 2050, and 2070, respectively.

4.2. Simulation of solute transport on the coastal aquifer salt mass

As mentioned earlier, the solute transport model SEAWAT was applied to identify the combined effect of SLR, reduction in the Nile River flow, and overpumping on aquifer salinity in the middle Nile aquifer. Also, different hydraulic conditions were implemented by decreasing the Nile hydrograph and increasing the abstraction rates in 2030, 2050, and 2070. The aquifer salt mass variation (SMV) $(C\text{-}C_0)/C_0$ was derived to monitor the evolution of the salt concentration within the aquifer (where C_0 is the initial salt concentration and C is the salt concentration for the given scenario). SWI was investigated by combining changes in the seawater heads by 17.60 cm, 32.20 cm, and 52.80 cm (Scenario A). Fig. 7b shows the vertical view for the distribution of TDS in the NDA in 2070 compared with Fig. 7a at the base case. The results indicated that increasing the hydrostatic pressure led to more saline intrusion into the aquifer, which induced a new shift in the freshwater-saltwater transition zone. The isochlorine at 35,000 ppm reached a distance of 64.20 km, 64.80 km, and 65.70 km, while it previously reached 102.50 km, 103.30 km, and 140.20 km at isochlorine 1000 in 2030, 2050, and 2070, respectively. The salt mass reached 28.34×10^4 tons per metre of shoreline (ton m^{-1}), 28.73×10^4 ton m^{-1}, and 29.06×10^4 ton m^{-1} for SLR in the years 2030, 2050, and 2070, respectively, while the initial 28.08×10^4 ton m^{-1} recorded in the base case. The aquifer salinity increased, and the SMV increased by 0.92%, 2.30%, and 3.48%.

SWI mechanism was then investigated by decreasing the Nile hydrograph and recharge (Scenario B) by 7.50%, 13%, and 18.50% from the baseline case in the years 2030, 2050, and 2070, respectively. The isochlorine at 35,000 ppm reached 66.90 km, 67.70 km, and 69 km, and the isochlorine at 1000 ppm reached 108.20 km, 109.40 km, and 110 km from the shoreline in the years 2030, 2050, and 2070, respectively (Fig. 7c). It is also relevant to note that reducing the Nile hydrograph increased the aquifer salinity. Moreover, the salt content increased up to 28.36×10^4 ton m^{-1}, 28.74×10^4 ton m^{-1}, and 29.07×10^4 ton m^{-1} following the decrease of the aquifer recharge, and the SMV increased by 0.99%, 2.33%, and 3.54%.

Scenario C considered the SWI response due to overpumping in the years 2030, 2050, and 2070, whereby the abstraction rates by production wells in the study area increased by 20%, 51%, and 92%, respectively, compared to the base case (Scenario C). Fig. 7d shows that the isochlorine 35,000 ppm reached a distance of 64.70 km, 65.10 km, and 65.50 km from the shoreline in 2030, 2050, and 2070, respectively, while the isochlorine 1000 ppm reached 106.50 km, 109.50 km, and 110.30 km from the shoreline at same years. The results evidence the significant effects of overpumping and land subsidence on the exacerbation of SWI in the aquifer. The salt content increased up to 29.62×10^4 ton m^{-1}, 30.15×10^4 ton m^{-1}, and 30.60×10^4 ton m^{-1} while the SMV increased by 5.49%, 7.38%, and 8.96%.

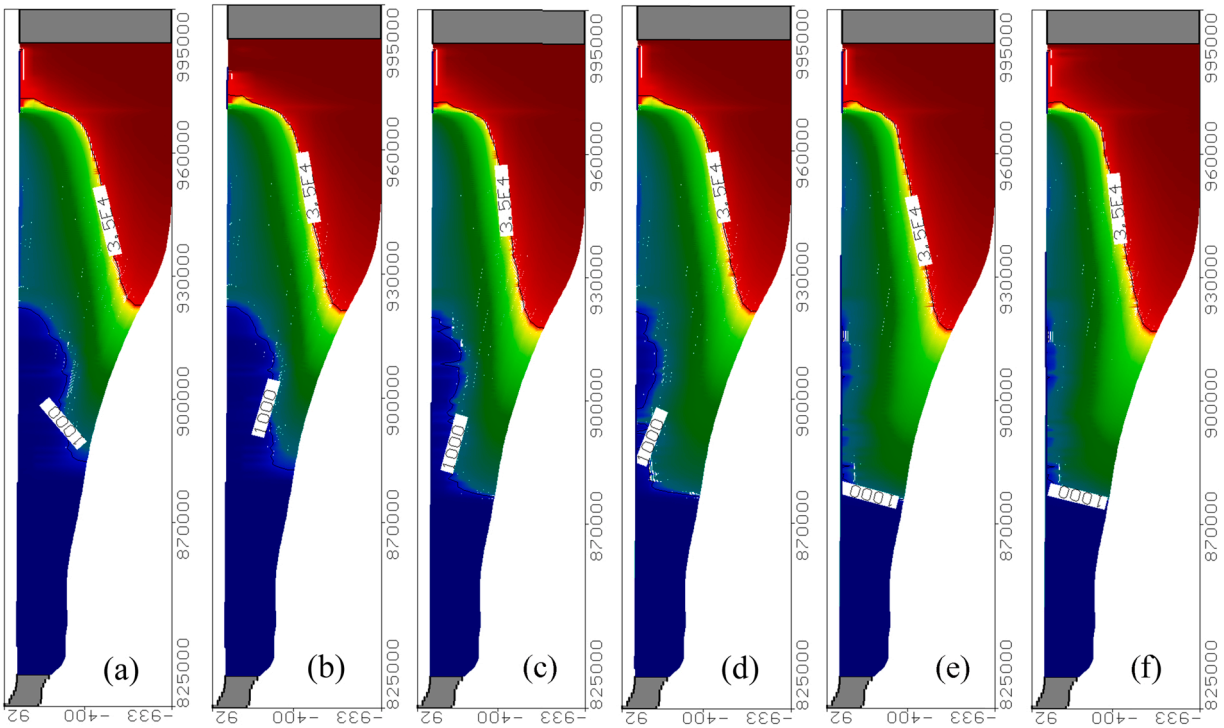

Fig. 7. Vertical section for the TDS in the investigated NDA for (a) base case, (b) future scenarios of SLR by 52.80 cm, (c) decreasing the flow to the aquifer by reduction in Nile River hydrograph by 18.50%, (d) increasing abstraction wells rates by 92%, (e) 18.50% reduction in Nile River hydrograph and 92% increasing abstraction wells rates, (f) 52.80 cm by SLR, 18.50% reduction in Nile hydrograph and 92% increasing abstraction.

Scenario D presents the response of SWI to the combined effects of decreasing the Nile hydrograph (Scenario B) and increasing the abstraction rate (Scenario C). Fig. 7e shows that the isochlorine 35,000 ppm and 1000 ppm reached 67.10 km, 68.90 km, 69.60 km and 109.20 km, 110.70 km, and 111.10 km from the shoreline, respectively, in 2030, 2050 and 2070. The results show that the reduction effect in the flow to the aquifer coupled with the increasing abstraction rates further increased SWI in coastal aquifers. In this scenario, an increase of the salt mass to 29.91 $\times$ 10^4 ton m^{-1}, 30.68 $\times$ 10^4 ton m^{-1}, and 31.14 $\times$ 10^4 ton m^{-1} and the SMV increased by 6.50%, 9.27%, and 10.89%.

Finally, in Scenario E, the aquifer salinity is investigated by increasing in sea-level (Scenario A), reducing the Nile hydrograph (Scenario B), and increasing the abstraction (Scenario C) in 2030, 2050, and 2070. Fig. 7f shows that the isochlorine 35,000 ppm reached 67.30 km, 69.10 km, 69.80 km, while and 1000 ppm reached 109.60 km, 110.80 km, and 112 km from the shoreline in the years 2030, 2050, and 2070, respectively. Also, increasing the saltwater head due to SLR combined with the reduction in the Nile River hydrograph, the return flow to the aquifer, and the overpumping by production wells resulted in the landward shifting of the saline water. In addition, this combined effect also caused the increase of the submerged area by seawater and land subsidence in the coastal aquifers. The aquifer salinity also increased significantly, resulting in a large quantity of freshwater deterioration. The salinity increased to 30.07 $\times$ 10^4 ton m^{-1}, 31.08 $\times$ 10^4 ton m^{-1}, and 31.73 $\times$ 10^4 ton m^{-1} for the years 2030, 2050, and 2070, respectively, and the SMV increased by 7.09%, 10.69%, and 12.99% (see Table 3).

4.3. Quantification of the impact on the future submarine groundwater discharge

The submarine groundwater discharge (SGD) due to SLR, reduction in the Nile River hydrograph, increase in abstraction rates of the production wells, and the combination of these factors was herein estimated. The submarine groundwater discharge variation (SGDV) $(Q\text{-}Q_0)/Q_0$ was derived from monitoring the evolution of the submarine groundwater discharge within the aquifer (where Q_0 is the initial submarine groundwater discharge and Q is the submarine groundwater discharge for the given scenario).

The study results show that these factors significantly impacted the NDA aquifer. A new value of SGD was predicted in the years 2030, 2050, and 2070. The recharge reached 1.20 cubic metres per day per metre of shoreline (m^3 day^{-1} m^{-1}) in the base case and decreased to 1.16 m^3 day^{-1} m^{-1}, 1.11 m^3 day^{-1} m^{-1}, and 1.07 m^3 day^{-1} m^{-1} in the years 2030, 2050, and 2070, respectively. Also, the reduction in SGDV was about 3.83%, 7.58%, and 11.24% as a consequence of the SLR of 17.60 cm, 32.20 cm, and 52.80 cm, respectively (Scenario A). Decreasing the Nile hydrograph (*Scenario B)* by 7.50%, 13%, and 18.50% compared with the base case reduced the SGD towards the sea by 1.11 m^3 day^{-1} m^{-1}, 1.05 m^3 day^{-1} m^{-1}, and 0.98 m^3 day^{-1} m^{-1}, which is equivalent to a reduction of SGDV reached 7.49%, 12.99%, and 18.65%. When the pumping rates of the production wells increased by 20%, 51%, and 92% compared with the base case (*Scenario C)*, it decreased the SGD to 1.06 m^3 day^{-1} m^{-1}, 0.87 m^3 day^{-1} m^{-1}, and 0.67 m^3 day^{-1} m^{-1}, which is equivalent to a reduction in the SGDV by 11.49%, 27.39%, and 44.30%. The combined effect in scenario D (*Scenario B combined with Scenario C)* led to a decrease in the SGD towards the sea by 0.98 m^3 day^{-1} m^{-1}, 0.76 m^3 day^{-1} m^{-1} and 0.54 m^3 day^{-1} m^{-1}, which the SGDV is equivalent to 18.48%, 36.47%, and 54.87%. Finally, *Scenario E* (Scenario A combined with Scenarios B and C) caused a decrease in the SGD towards the sea to 0.94 m^3 day^{-1} m^{-1}, 0.69 m^3 day^{-1} m^{-1}, and 0.46 m^3 day^{-1} m^{-1}, which the SGDV is equivalent to a decrease of 21.90%, 42.38%, and 61.95% in the years 2030, 2050, and 2070 respectively (see Fig. 8a).

The numerical modelling results reveal that increasing the sea level, reducing the flow to the aquifer due to reduction in Nile hydrograph, and increasing abstraction rates has noticeably decreased the freshwater discharge towards the sea, and subsequently causing further intrusion of saline water in the middle NDA aquifer, as shown in Fig. 8b.

Table 3
SWI results for the investigated future scenarios.

Scenarios	Case	Year	Value	Intrusion length (km)		Salt mass	
				3500	1000	(t/m) x 10^4	%
	Base	2008	-	63.60	101.70	28.08	-
A	Seal level rise (cm)	2030	7.62 cm	64.20	102.50	28.34	0.92
		2050	35.6 cm	64.80	103.30	28.73	2.30
		2070	52.8 cm	65.70	104.20	29.06	3.48
B	Reduction in Nile River hydrograph with return flow	2030	7.50%	67	108.20	28.36	5.49
		2050	13%	67.70	109.40	28.74	7.38
		2070	18.5%	69	110	29.07	8.96
C	Increasing abstraction wells rates	2030	21%	64.70	106.50	29.62	0.99
		2050	52%	65.10	109.50	30.15	2.33
		2070	92%	65.50	110.30	30.60	3.54
D	Recharge in Nile River hydrograph with recharge return flow and increasing abstraction	2030	combine values in scenarios B,	67.10	109.20	29.91	6.50
		2050	and C	68.90	110.70	30.68	9.27
		2070		69.60	111.10	31.14	10.89
E	SLR, recharge Reduction and increasing abstraction	2030	combine values in scenarios	67.30	109.60	30.07	7.09
		2050	A, B and C	69.10	110.80	31.08	10.69
		2070		69.80	112	31.73	12.99

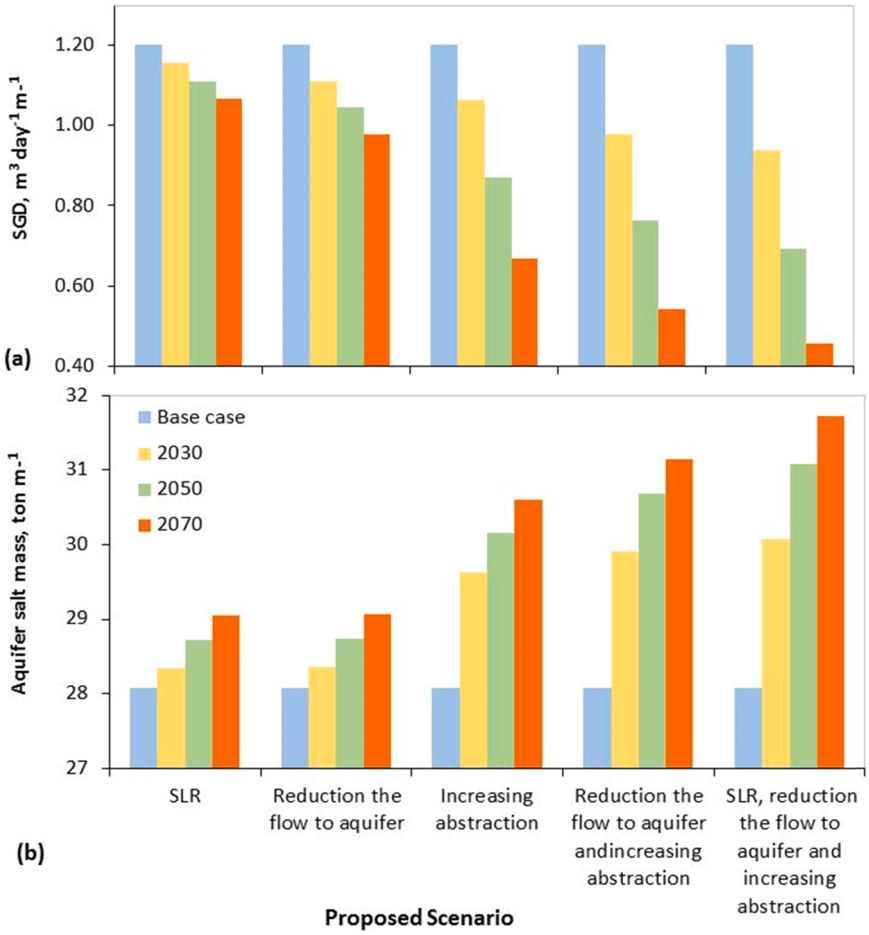

Fig. 8. Nile delta at different scenarios for (a) submarine groundwater discharge (SGD) and (b) aquifer salt mass.

5. Conclusions

Groundwater resources in coastal regions are susceptible to climate change and freshwater demand, which will increase due to overpopulation, especially in arid and semi-arid regions. Numerical modelling was used to analyse the main factors, including the hydrogeological and anthropogenic factors, on the submarine groundwater discharge (SGD) and saltwater intrusion in the Nile Delta aquifer, Egypt. The main factors investigated included sea-level rise, reduction in River Nile hydrograph, increasing groundwater pumping, and a combination of these scenarios.

The results show that the groundwater levels along the coastline noticeably increased when the sea level increased (Scenarios.1) by 17.60 cm, 32.20 cm and 52.80 cm compared with the base case. The aquifer salt mass variation (SMV) increased to 0.92%, 2.30% and 3.48% compared to the base case. Moreover, the submarine groundwater discharge variation (SGDV) decreased by 3.83%, 7.58% and 11.24% in the years 2030, 2050 and 2070, respectively. Moreover, the inland groundwater heads decreased noticeably following the reduction of the Nile flow (Scenarios.2) by 7.50%, 13% and 18.50%. The SMV increased by 5.49%, 7.38% and 8.96%, and the SGDV towards the sea declined by 7.49%, 12.99% and 18.65%, respectively. Increasing the abstraction (Scenarios.3) by 20%, 51% and 92% induced a decrease in the groundwater heads, and the SMV was increased by 0.99%, 2.33%, and 3.54%. In addition, the SGDV decreased by 11.49%, 27.39%, and 44.30%, respectively. Combining the effect of reducing the Nile flow hydrograph and sea recharge with excessive pumping (Scenarios D) caused the SMV to increase by 6.50%, 9.27%, and 10.89% and the SGDV towards the sea to decrease by 18.48%, 36.47%, and 54.87%, respectively. Finally, the combination of scenarios A, B, and C (Scenarios E) caused a decrease in the groundwater heads and an increase of the SMV by 7.09%, 10.69%, and 12.99%. Scenario E also exhibited a decrease of the SGDV towards the sea by 21.90%, 42.38%, and 61.95% in the years 2030, 2050, and 2070, respectively.

The study emphasises the importance of adequate and effective fresh groundwater resources to manage the submarine groundwater discharge directly to the sea and control the groundwater salinity in order to enable optimal and sustainable use of the fresh groundwater in the region.

Ethics approval

Not applicable.

Funding

This study did not receive any funding.

CRediT authorship contribution statement

Ismail Abd-Elaty, Antoifi Abdoulhalik, and Ashraf Ahmed: Conceptualization, Methodology, Investigation, Formal analysis, Data curation. **Ismail Abdelaty, Antoifi Abdoulhalik, and Ashraf Ahmed**: Visualization, Writing – original draft, Writing – review & editing, Resources. **Ashraf Ahmed**: Supervision.

Declaration of Competing Interest

The authors declare that they have no known competing financial interests or personal relationships that could have appeared to influence the work reported in this paper.

Data availability

No data was used for the research described in the article.

Acknowledgement

The authors thank the Department of Water and Water Structures Engineering, Faculty of Engineering, Zagazig University, Zagazig 44519, Egypt, for constant support during the study.

Code availability

Upon request.

Consent to participate

Yes.

Consent for publication

Yes.

Appendix A. Supporting information

Supplementary data associated with this article can be found in the online version at doi:10.1016/j.ejrh.2023.101395.

References

Abd-Elaty, I. (2014). Numerical and Experimental Study for Simulating Climatic Changes Effects on Nile Delta Aquifer (PhD Thesis), Faculty of Engineering, Zagazig University, Egypt.

Abd-Elaty, I., Zelenakova, M., 2022. Saltwater intrusion management in shallow and deep coastal aquifers for high aridity regions. J. Hydrol. Reg. Stud. 40, 101026 https://doi.org/10.1016/j.ejrh.2022.101026.

Abd-Elaty, I., Polemio, M., 2023. Saltwater intrusion management at different coastal aquifers bed slopes considering sea level rise and reduction in fresh groundwater storage. Stoch. Environ. Res Risk Assess. https://doi.org/10.1007/s00477-023-02381-9.

Abd-Elaty, I., Straface, S., Kuriqi, A., 2021a. Sustainable saltwater intrusion management in coastal aquifers under climatic changes for humid and hyper-arid regions. Ecol. Eng. 171 https://doi.org/10.1016/j.ecoleng.2021.106382.

Abd-Elaty, I., Sallam, G., Strafacec S, A., Scozzari, A., 2019. Effects of climate change on the design of subsurface drainage systems in coastal aquifers in arid/semi-arid regions: case study of the Nile delta. Sci. Total Environ. J. 672, 283–295. https://doi.org/10.1016/j.scitotenv.2019.03.483.

Abd-Elaty, I., Saleh, O.K., Ghanayem, H.M., Grischek, T., Zelenakova, M., 2021b. Assessment of hydrological, geohydraulic and operational conditions at a riverbank filtration site at Embaba, Cairo using flow and transport modeling. J. Hydrol. Reg. Stud. 37, 100900 https://doi.org/10.1016/j.ejrh.2021.100900.

Abd-Elaty, I., Kushwaha, N.L., Grismer, M.E., Elbeltagi, A., Kuriqi, A., 2022a. Cost-effective management measures for coastal aquifers affected by saltwater intrusion and climate change. Sci. Total Environ. 836, 155656 https://doi.org/10.1016/j.scitotenv.2022.155656.

Abd-Elaty, I., Pugliese, L., Bali, K.M., Grismer, M.E., Eltarabily, M.G., 2022b. Modelling the impact of lining and covering irrigation canals on underlying groundwater stores in the Nile Delta, Egypt. Hydrol. Process. 36, e14466 https://doi.org/10.1002/hyp.14466.

Abd-Elaty, Ismail, Martina Zeleňáková, Katarína Krajníková, Hany, F.Abd-Elhamid, 2021c. Analytical solution of saltwater intrusion in costal aquifers considering climate changes and different boundary conditions. Water 13 (7), 995. https://doi.org/10.3390/w13070995.

Abdoulhalik, A., Ahmed, A.A., 2018. Transient investigation of saltwater upconing in laboratory-scale coastal aquifer. Estuar. Coast. Shelf Sci. 214, 149–160. https://doi.org/10.1016/j.ecss.2018.09.024.

Abdoulhalik, A., Abdelgawad, A.M., Ahmed, A.A., 2020. Impact of layered heterogeneity on transient saltwater upconing in coastal aquifers. J. Hydrol. 581, 124393.

Amary W. (2008) Study the Sedimentation Inside High Aswan Dam Reservoir (M.Sc. thesis), Faculty of Engineering, Cairo University, Egypt.

Darwish, M.M. (1994) Effect of Probable Hydrological Changes on the Nile Delta Aquifer System (Ph.D. Thesis), Faculty of Engineering, Cairo University, Cairo, Egypt.

El Shinawi, A., Kuriqi, A., Zelenakova, M., Vranayova, Z., Abd-Elaty, I., 2022. Land subsidence and environmental threats in coastal aquifers under sea level rise and over-pumping stress. J. Hydrol. 608, 127607 https://doi.org/10.1016/j.jhydrol.2022.127607.

El-Fayoumi, L.F. (1968) Geology of Groundwater Supplies in the Eastern Region of the Nile Delta and Its Extension in the North Sinai (PhD. thesis), Cairo University, Egypt.

Engelen, J.V., Verkaik, J., King, J., Nofal, E.R., Bierkens, M.F.P., Oude Essink, G.H.P., 2019. A three-dimensional palaeohydrogeological reconstruction of the groundwater salinity distribution in the Nile Delta Aquifer. Hydrol. Earth Syst. Sci. 23, 5175–5198. https://doi.org/10.5194/hess-23-5175.

Guo W., Langevin C.D. (2002) User's guide to SEAWAT; a computer program for simulation of three-dimensional variable-density groundwater flow.

Harbaugh, A.W., Banta, E.R., Hill, M.C., and McDonald, M.G., (2000), MODFLOW-2000, the US Geological Survey Modular Groundwater Model—User guide to modularisation concepts and the groundwater flow process: US Geological Survey Open-File Report 00-92, 121 p.

Hefny, K.H., (1980) Groundwater in the Nile Valley, Ministry of Irrigation, Water Research Center. Groundwater Research inst. pp. 1–120.

Hossen, Hickmat, Nour-Eldeen, A.S., Negm, Abdelazim, Hamdan, Ali M., Elsahabi, Mohamed, Zelenakova, Martina, Abd-Elaty, Ismail, 2022. Investigation of groundwater logging for possible changes in recharge boundaries and conditions in the City of Aswan, Egypt. Water 14 (7), 1164. https://doi.org/10.3390/w14071164.

IPCC (2008) Climate Change and Water‖, Technical Paper of the Intergovernmental Panel on Climate Change, edited by: Bates, B. C., Kundzewicz, Z. W., Wu, S., and Palutikof, J. P., IPCC Secretariat, Geneva, p. 210.

IPCC, 2014. Summary for policy makers. In: Field, C.B., Barros, V.R., Dokken, D.J., Mach, K.J., Mastrandrea, M.D., Bilir, T.E., Chatterjee, M., Ebi, K.L., Estrada, Y.O., Genova, R.C., Girma, B., Kissel, E.S., Levy, A.N., MacCracken, S., Mastrandrea, P.R., White, L.L. (Eds.), Climate Change 2014: Impacts, Adaptation, and Vulnerability. Synthesis Report Based on the Contribution of the Three Working Groups to the Fifth Assessment Report of the Intergovernmental Panel on Climate Change. Cambridge University Press, Cambridge, United Kingdom and New York, NY, USA, pp. 1–32.

Langevin, C.D., Thorne Jr., D.T., Dausman, A.M., Sukop, M.C., Guo, Weixing, 2007. SEAWAT Version 4: A computer program for simulation of multi-species solute and heat transport: US Geological Survey Techniques and Methods, book 6, chap. A22 39.

Legeais, J.-F., Ablain, M., Zawadzki, L., Zuo, H., Johannessen, J.A., Scharffenberg, M.G., Fenoglio-Marc, L., Fernandes, M.J., Andersen, O.B., Rudenko, S., Cipollini, P., Quartly, G.D., Passaro, M., Cazenave, A., Benveniste, J., 2018. An improved and homogeneous altimeter sea-level record from the ESA Climate Change Initiative. Earth Syst. Sci. Data 10, 281–301. https://doi.org/10.5194/essd-10-281-2018.

Mabrouk, M.B., Jonoski, A., Solomatine, D., Uhlenbrook, S., 2013. A review of seawater intrusion in the Nile Delta groundwater system–the basis for assessing impacts due to climate changes and water resources development. Hydrology and Earth System Sciences Discussions 10 (8), 10873–10911.

Mabrouk, Marmar, Jonoski, Andreja, Essink, Oude, Gualbert, H.P., Uhlenbrook, Stefan, 2019. Assessing the fresh–saline groundwater distribution in the Nile Delta Aquifer using a 3D variable-density groundwater flow model. Water 11 (9), 1946. https://doi.org/10.3390/w11091946.

Ministry of Water Resources and Irrigation (MWRI) (2013) Proposed Climate Change Adaptation Strategy for the Ministry of Water Resources and Irrigation in Egypt, Ministry of Water Resources and Irrigation.

Molle F., Gaafar I., El-Agha D.E., Rap E. (2016) Irrigation Efficiency and the Nile Delta Water Balance, Water and salt management in the Nile Delta: Report No. 9, International water management institute and Australian Center for International Agriculture Research.

Morsy, W.S. (2009) Environmental Management to Groundwater Resources for Nile Delta Region (PhD thesis), Faculty of Engineering, Cairo University, Egypt.

Nasar, M.K.K. (2004) Design and Management of Discharge and Recharge Well Field for Coastal Desalination Plants (MSc. thesis), Cairo University, Egypt.

Negm, A.M., Sakr, S., Abd-Elaty, I., Abd-Elhamid, H.F., 2018. An overview of groundwater resources in Nile Delta Aquifer. In: Negm, A. (Ed.), Groundwater in the Nile Delta, The Handbook of Environmental Chemistry, vol. 73. Springer, Cham. https://doi.org/10.1007/698_2017_193.

Nerem, R.S., Beckley, B.D., Fasullo, J.T., Hamlington, B.D., Masters, D., Mitchum, G.T., 2018. Climate-change–driven accelerated sea-level rise detected in the altimeter era. Proc. Natl. Acad. Sci. USA, 201717312 https://doi.org/10.1073/pnas.1717312115.

Nofal, E.R., Amer, M.A., El-Didy, S.M., Fekry, A.M., 2015. Delineation and modeling of seawater intrusion into the Nile Delta Aquifer: a new perspective. Water Sci. 29 (2), 156–166.

Radwan, T.M., Blackburn, G.A., Whyatt, J.D., Atkinson, P.M., 2019. Dramatic loss of agricultural land due to urban expansion threatens food security in the Nile Delta, Egypt. Remote Sens. 11, 332 ([Google Scholar] [CrossRef]).

Ramadan, S., Negm, A.M., Smanny, M., and Helmy, A. (2015) Quantifying the impacts of impounding grand Ethiopian renaissance dam reservoir on Nasser lake active storage. In: Proceedings of Eighteenth International Water Technology Conference (IWTC 18), Sharm El Sheikh, 12–14.

RIGW, (2002) Nile Delta Groundwater Modeling Report, Research Inst. for Groundwater, Kanater El-Khairia, Egypt, 2002.

RIGW (Research Institute for Groundwater), 1966. Groundwater research along the Nile River. Ministry of Irrigation, Arab Republic of Egypt.

RIGW (Research Institute for Groundwater), IGW, (1992) Hydrogeological Map of Nile Delta, Scale 1: 500,000, first ed, Nile Delta, Research Inst. for Groundwater, Kanater El-Khairia, Egypt, 1992.

Sakr, S.A., Attia, F.A., Millette, J.A., 2004. Vulnerability of the Nile Delta aquifer of Egypt to seawater intrusion. In: *International conference on water resources of arid and semi-arid regions of Africa, Issues and challenges*. Gaborone, Botswana. August.

Saleh, W.S.M., 2009. Environmental Management of Groundwater Resources in the Nile Delta Region (Ph.D. thesis), Cairo University, Egypt.

Sallouma, M.K.M., 1983. Hydrogeological and Hydrochemical Studies East of Nile Delta, Egypt (Ph.D. Thesis), Ain Shams University.

Sestini, G., 1989. Nile Delta: a review of depositional environments and geological history. In: Whateley, M.K.G., Pickering, K.T. (Eds.), Deltas: Sites and Traps for Fossil Fuels. Geol. Soc. Spec. Publ., 41, pp. 99–127.

Wassef, R., Schüttrumpf, H., 2016. Impact of sea-level rise on groundwater rsalinity at the development area western delta, Egypt. Groundw. Sustain. Dev. 2–3, 85–103.

Wilson, J., Townley, H., Sada, C.A., 1979. Mathematical development and verification of a finite element aquifer flow model AQUIFEM-1. In: Technology Adaptation PRPGRAM Report No. 79-2. MIT, Cambridge.

Zheng, C., Wang, P.P., 1999. MT3DMS: a modular three-dimensional multispecies transport model for simulation of advection, dispersion, and chemical reactions of contaminants in groundwater systems; documentation and user's guide.